Supplementary Information

Origin of high thermoelectric performance with wide range of compositions for $Bi_xSb_{2-x}Te_3$ single quintuple layer

Zhen Li,[a] Siyu Han,[a] Yuanchun Pan,[a] Naihua Miao, [ab] Jian Zhou, [*a] Huibin Xu, [a] and Zhimei Sun[*ab]

[a] *School of Materials Science and Engineering and Beihang University, Beijing 100191, China*

[b] *Center for Integrated Computational Materials Engineering, International Research Institute for Multidisciplinary Science, Beihang University, Beijing 100191, China*

E-mail: jzhou@buaa.edu.cn, zmsun@buaa.edu.cn

1. The disorder geometry used for the BST systems.

For a structure with n dopant atoms, we have used the randomly distributed n-th dopant atom in the substitutional positions with the same distributions as that of $n - 1$ dopant atoms. Taking the $BiSbTe_3$ single QL as an example, the structure is shown in Fig. S1(a). We have also considered the SQS model, as shown in Fig. S1(b). To check the reliability of the structure used in this work, the total energy of the both models are calculated and compared. For the $BiSbTe_3$ single QL, it turns out that the total energy of the "random n-th" model is -3664.77 meV/atom, while that of the SQS model is -3664.50 meV/atom. The difference between the two random models is 0.27 meV/atom. Thus, the disorder geometry used for the BST systems in this work is reliable and consistent with the SQS model.

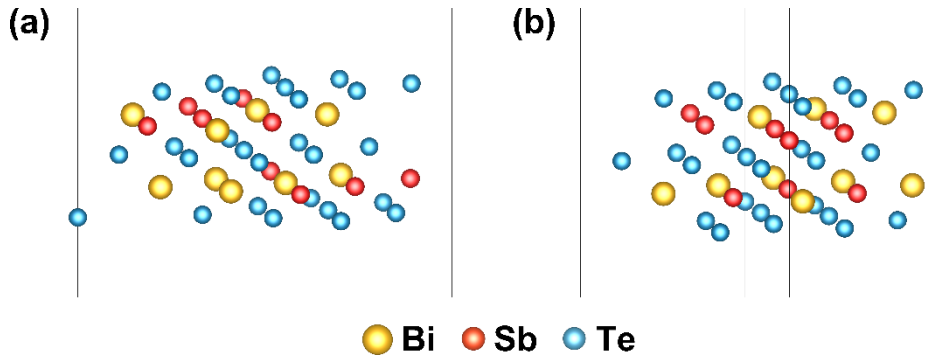

Figure S1 (a) The "random n-th" model and (b) the SQS model for $BiSbTe_3$ single quintuple layer.

2. The unfolded band structures of BST single QLs with different compositions simulated using the supercell.

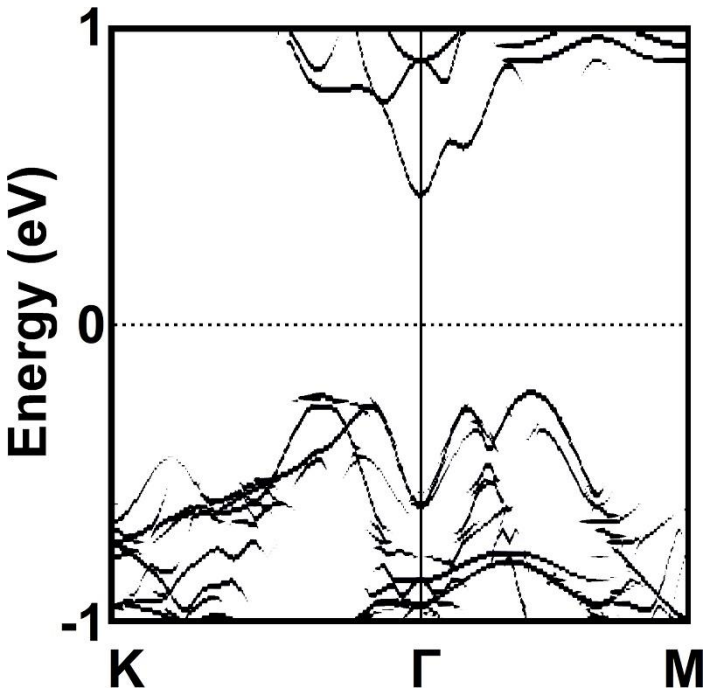

Figure S2 Unfolded band structure for single QL of $Bi_{0.111}Sb_{1.889}Te_3$.

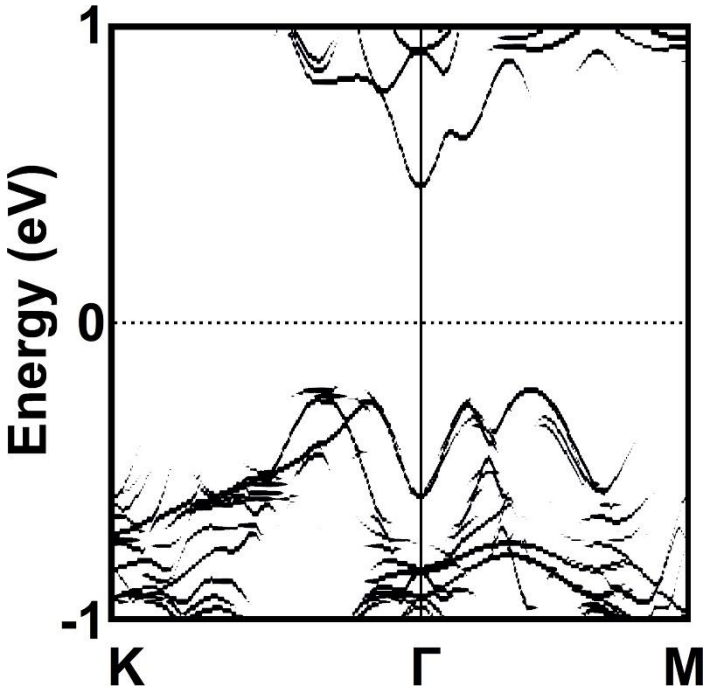

Figure S3 Unfolded band structure for single QL of $Bi_{0.167}Sb_{1.833}Te_3$

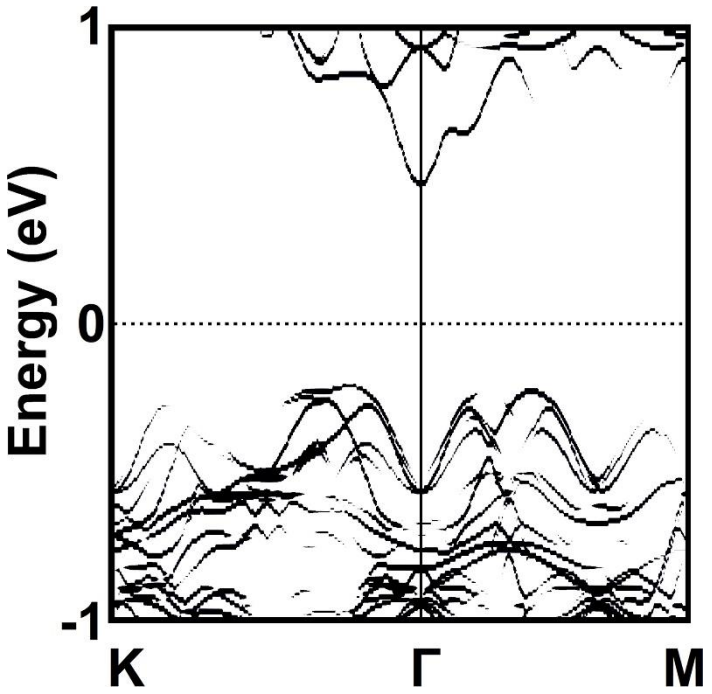

Figure S4 Unfolded band structure for single QL of $Bi_{0.222}Sb_{1.778}Te_3$

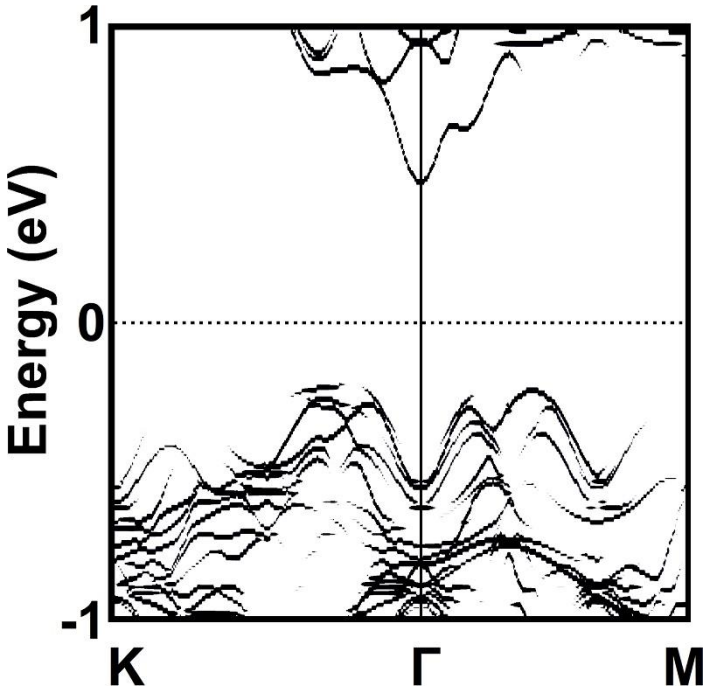

Figure S5 Unfolded band structure for single QL of $Bi_{0.278}Sb_{1.722}Te_3$

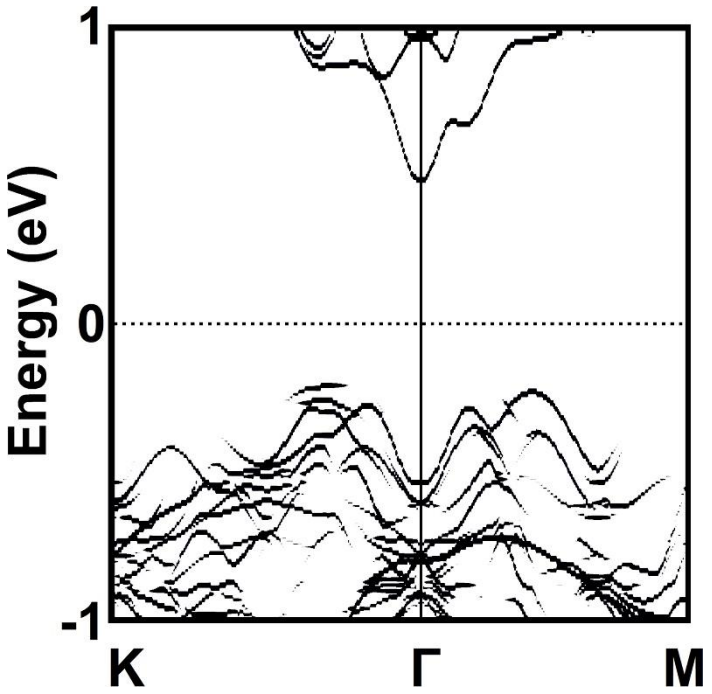

Figure S6 Unfolded band structure for single QL of $Bi_{0.333}Sb_{1.667}Te_3$

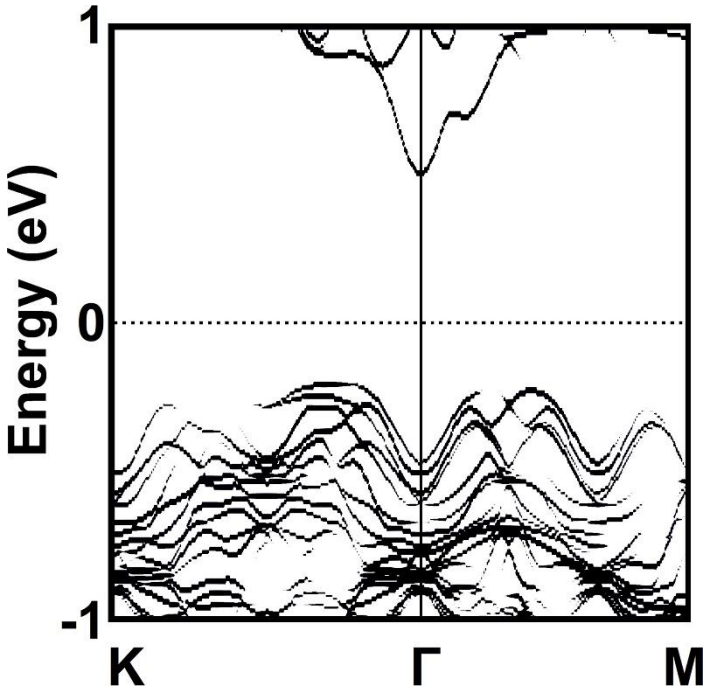

Figure S7 Unfolded band structure for single QL of $Bi_{0.389}Sb_{1.611}Te_3$

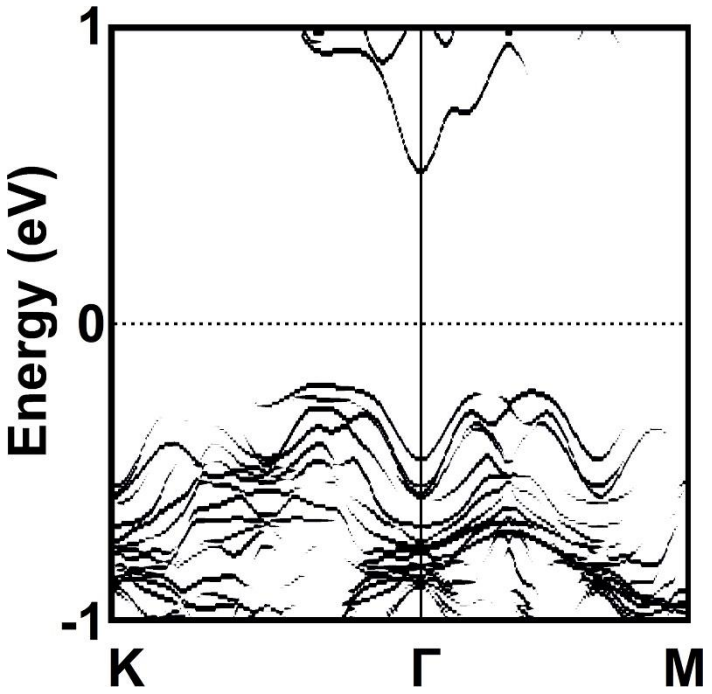

Figure S8 Unfolded band structure for single QL of $Bi_{0.444}Sb_{1.556}Te_3$

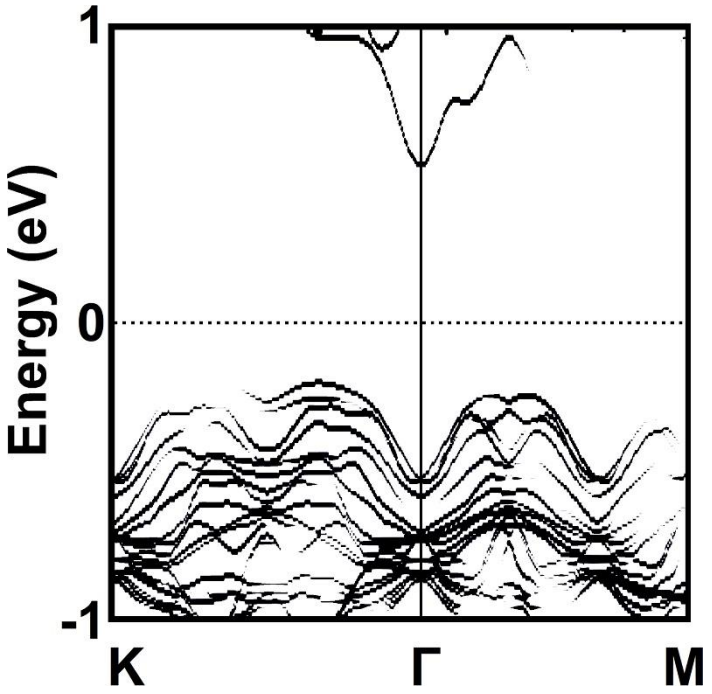

Figure S9 Unfolded band structure for single QL of $Bi_{0.556}Sb_{1.444}Te_3$

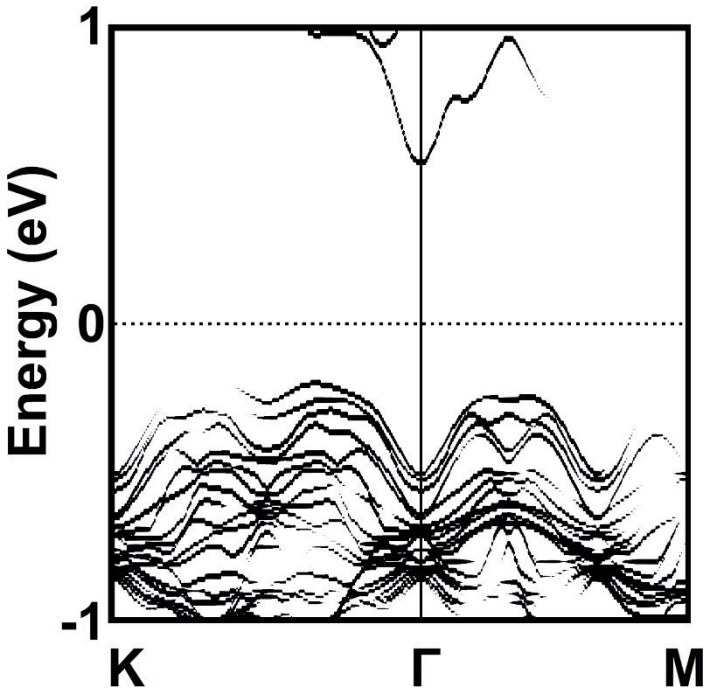

Figure S10 Unfolded band structure for single QL of $Bi_{0.611}Sb_{1.389}Te_3$

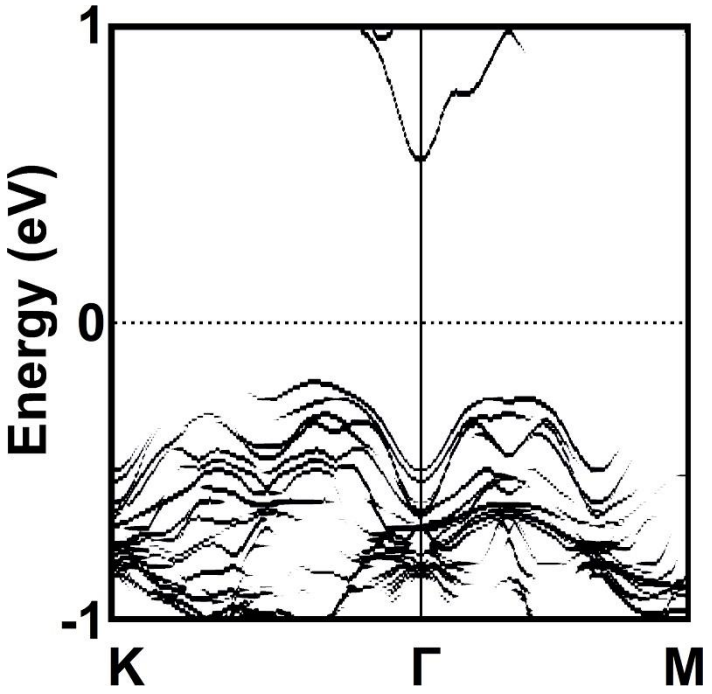

Figure S11 Unfolded band structure for single QL of $Bi_{0.667}Sb_{1.333}Te_3$

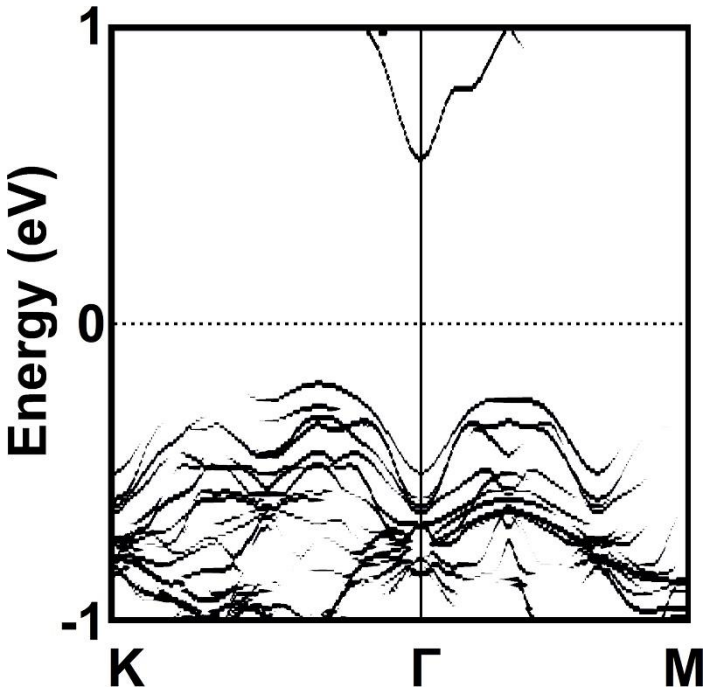

Figure S12 Unfolded band structure for single QL of $Bi_{0.722}Sb_{1.278}Te_3$

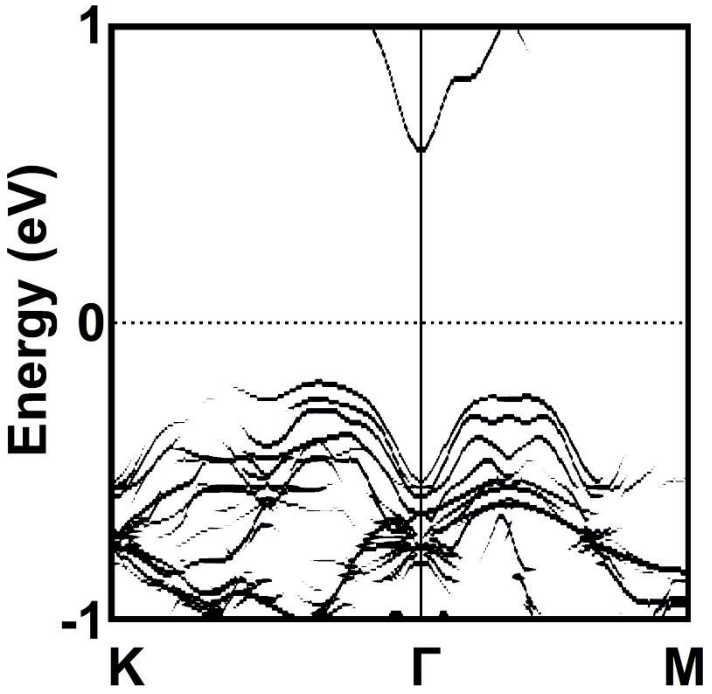

Figure S13 Unfolded band structure for single QL of $Bi_{0.778}Sb_{1.222}Te_3$

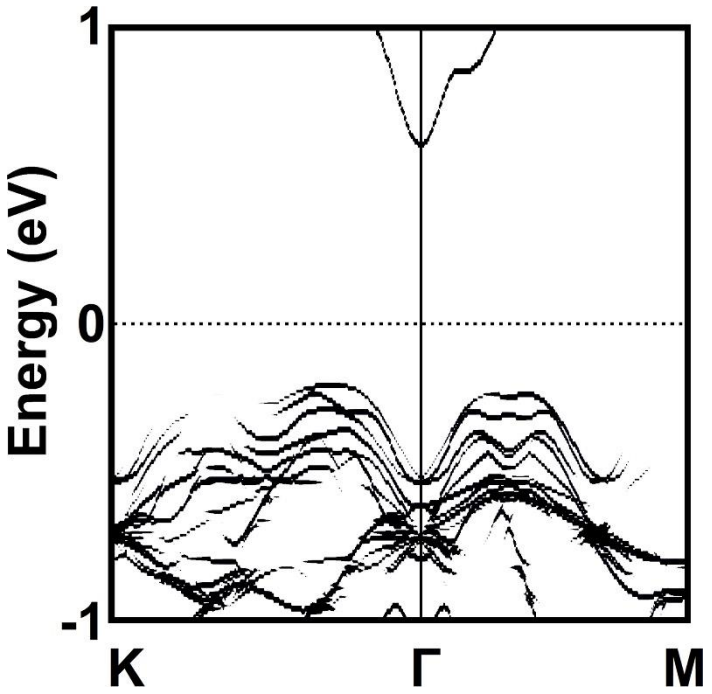

Figure S14 Unfolded band structure for single QL of $Bi_{0.833}Sb_{1.167}Te_3$

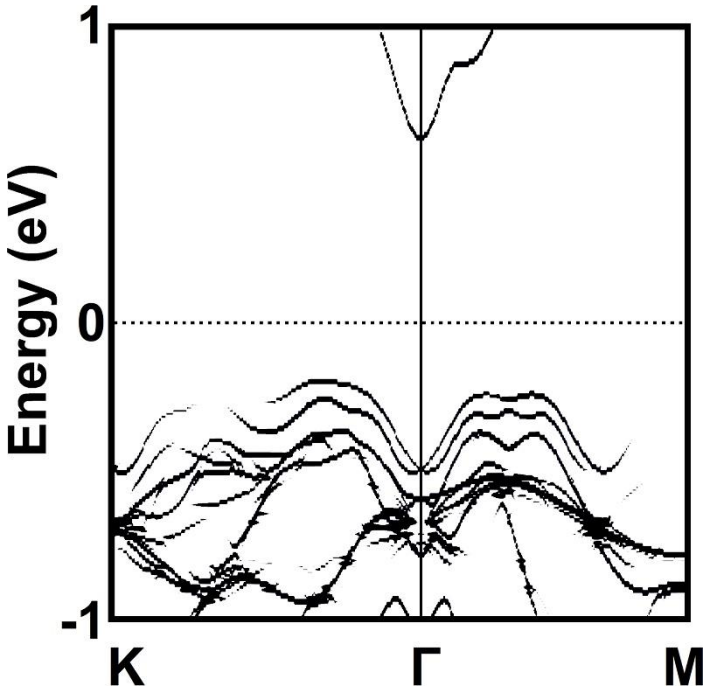

Figure S15 Unfolded band structure for single QL of $Bi_{0.889}Sb_{1.111}Te_3$

3. Band structure of $BiSbTe_3$ single quintuple layer with and without SOC.

The spin orbit coupling (SOC) may have some effects on the BST ones as Bi is a heavy element. We have calculated and compared the band structure of the $BiSbTe_3$ single quintuple layer with and without SOC, as shown in Fig. S16. It can be seen that SOC has very little effect on the shape of valance bands, especially for the valance bands near the Fermi energy, while the conductive bands are affected. Considering that the properties of *p*-type semiconductors are determined by the valance bands, the performance of *p*-type BST system in this work would show little difference with and without SOC.

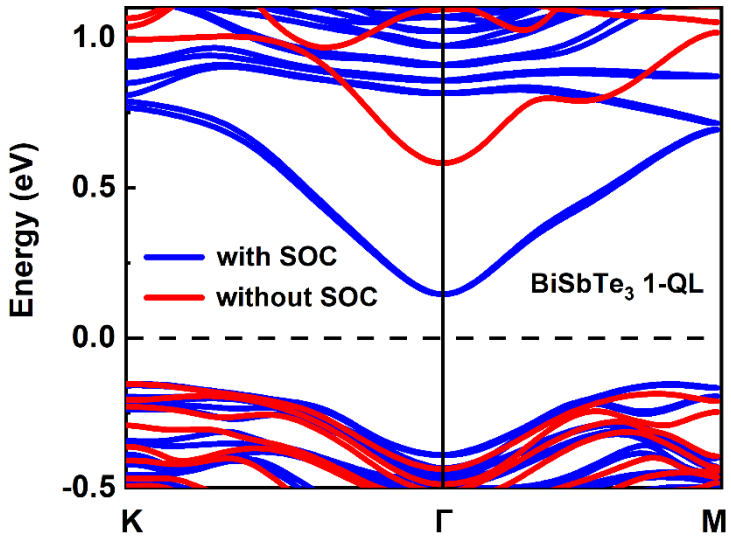

Figure S16 Band structure of $BiSbTe_3$ single quintuple layer with and without SOC.

4. Electronic transport properties of *p*-type $BiSbTe_3$ single quintuple layer with and without SOC.

Based on the calculated band structures, the calculated electronic transport properties of $BiSbTe_3$ single quintuple layer with and without SOC are shown in Fig. S17. It is shown that at condition of *p*-type conduction, there would be little difference between the Seebeck coefficient and electronic conductivity with and without SOC, which is consistent with the little change of the valance bands in the band structure.

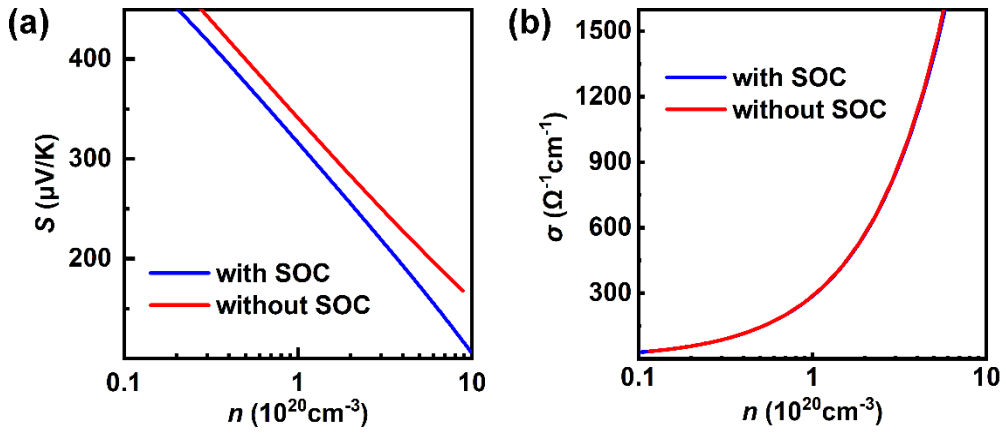

Figure S17 (a) Seebeck coefficient and (b) electronic conductivity of *p*-type $BiSbTe_3$ single quintuple layer with and without SOC.

5. The relaxation time used for BST single QLs.

Table S1 The relaxation time used for BST single QLs with different compositions.

Composition	relaxation time (fs)
Sb_2Te_3	12
$Bi_{0.111}Sb_{1.889}Te_3$	12.556
$Bi_{0.222}Sb_{1.778}Te_3$	13.111
$Bi_{0.333}Sb_{1.667}Te_3$	13.667
$Bi_{0.444}Sb_{1.556}Te_3$	14.222
$Bi_{0.556}Sb_{1.444}Te_3$	14.778
$Bi_{0.667}Sb_{1.333}Te_3$	15.333
$Bi_{0.778}Sb_{1.222}Te_3$	15.889
$Bi_{0.889}Sb_{1.111}Te_3$	16.444
$Bi_1Sb_1Te_3$	17
$Bi_{1.111}Sb_{0.889}Te_3$	17.556
$Bi_{1.222}Sb_{0.778}Te_3$	18.111
$Bi_{1.333}Sb_{0.667}Te_3$	18.667
$Bi_{1.444}Sb_{0.555}Te_3$	19.222
$Bi_{1.556}Sb_{0.444}Te_3$	19.778
$Bi_{1.667}Sb_{0.333}Te_3$	20.333
$Bi_{1.778}Sb_{0.222}Te_3$	20.889
$Bi_{1.889}Sb_{0.111}Te_3$	21.444
Bi_2Te_3	22

6. The partial density of states (PDOS) for different elements of BST single QLs.

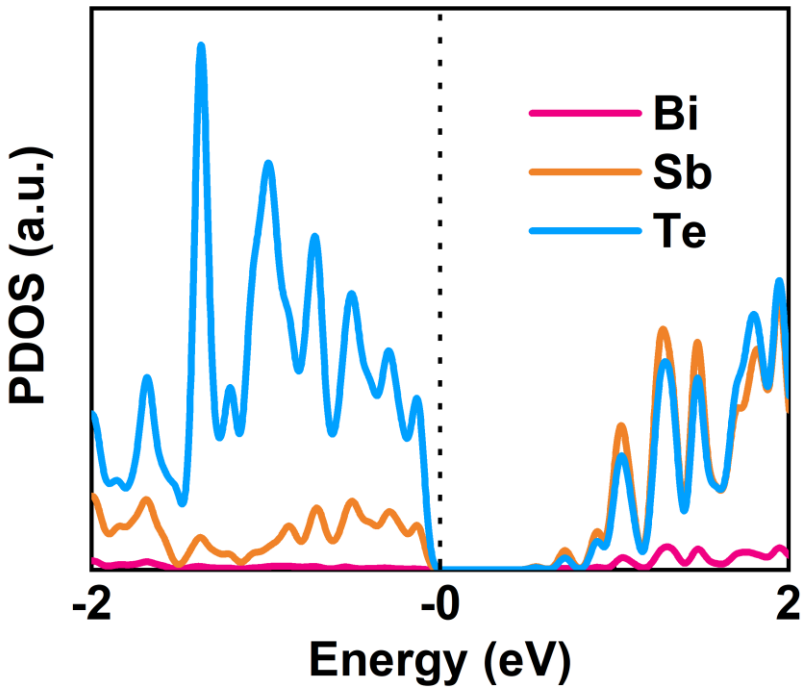

Figure S18 PDOS for $Bi_{0.111}Sb_{1.889}Te_3$.

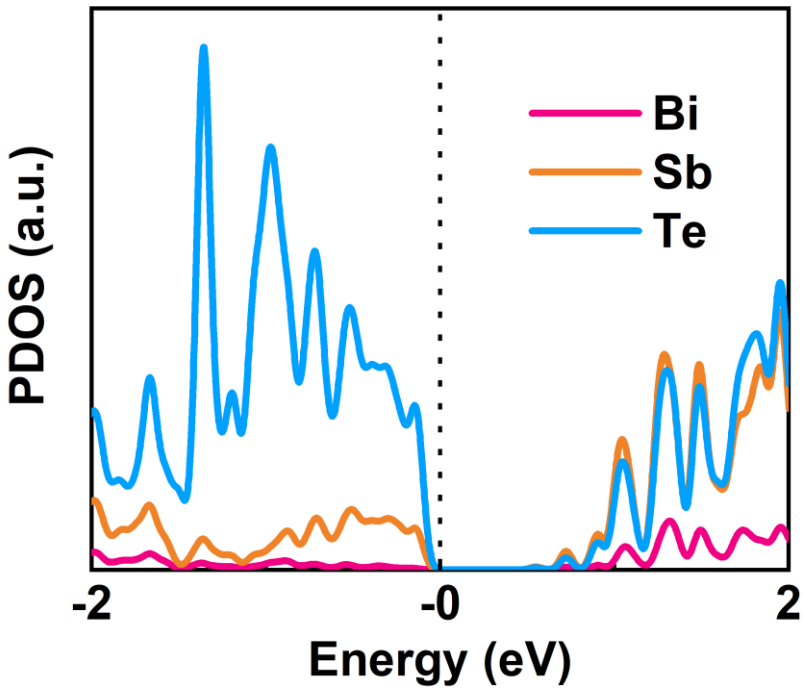

Figure S19 PDOS for $Bi_{0.222}Sb_{1.778}Te_3$.

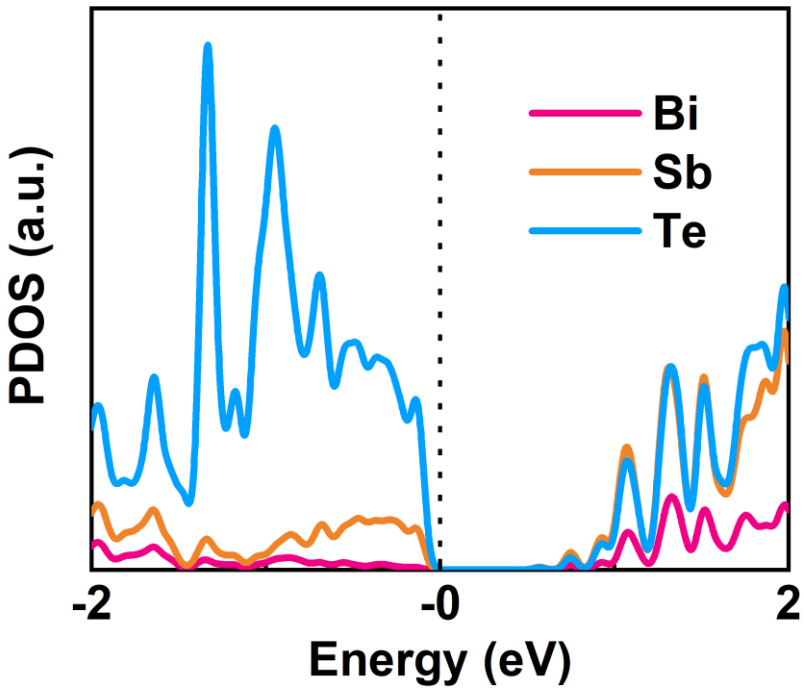

Figure S20 PDOS for $Bi_{0.333}Sb_{1.667}Te_3$.

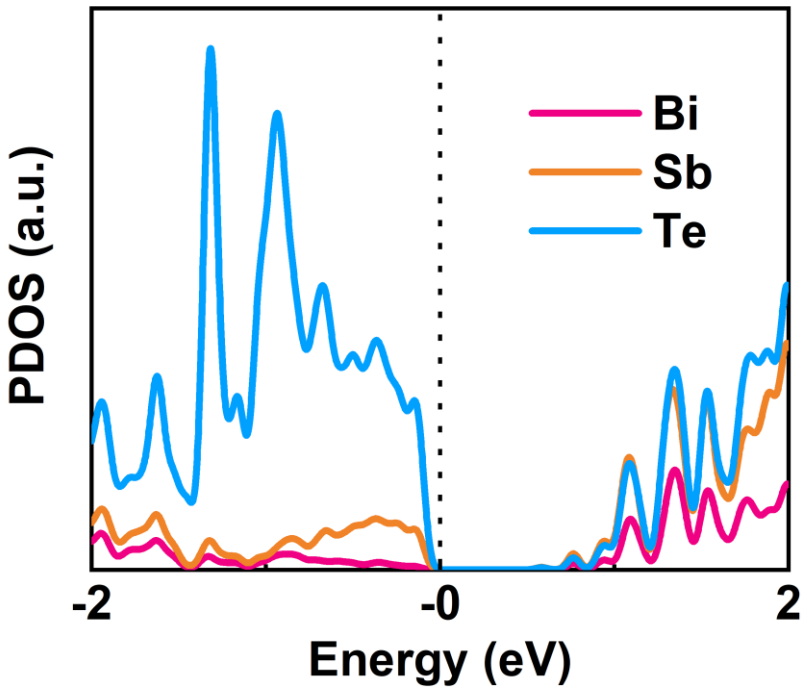

Figure S21 PDOS for $Bi_{0.444}Sb_{1.556}Te_3$.

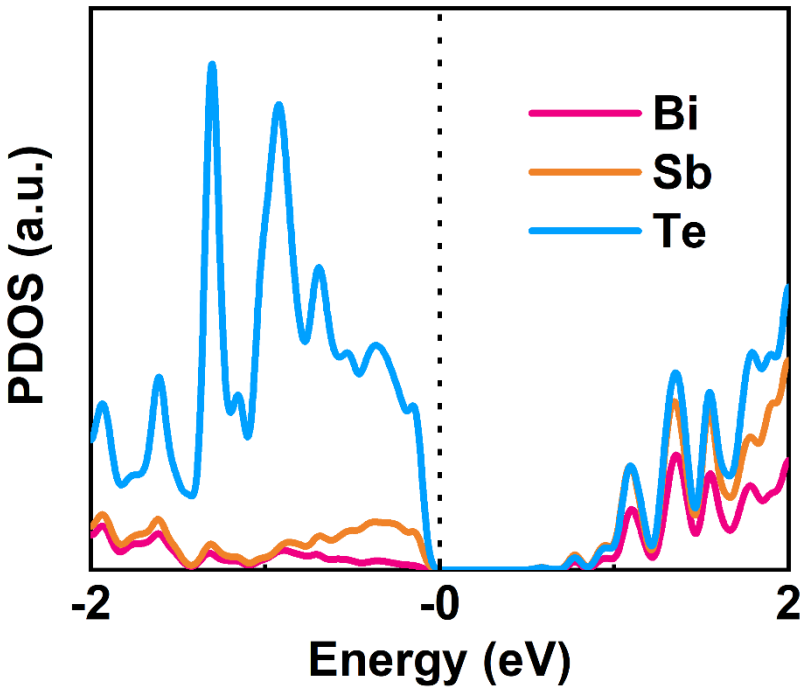

Figure S22 PDOS for $Bi_{0.556}Sb_{1.444}Te_3$.

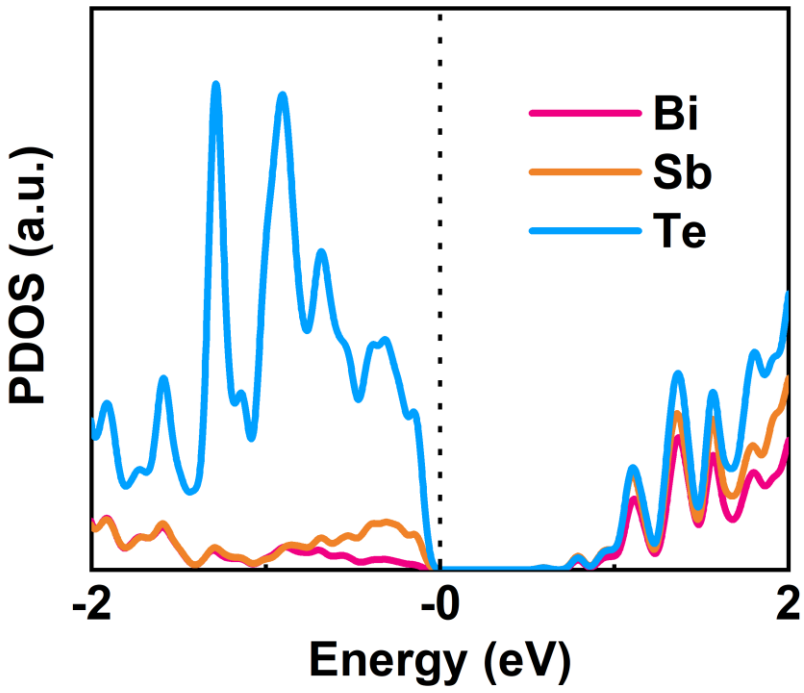

Figure S23 PDOS for $Bi_{0.667}Sb_{1.333}Te_3$.

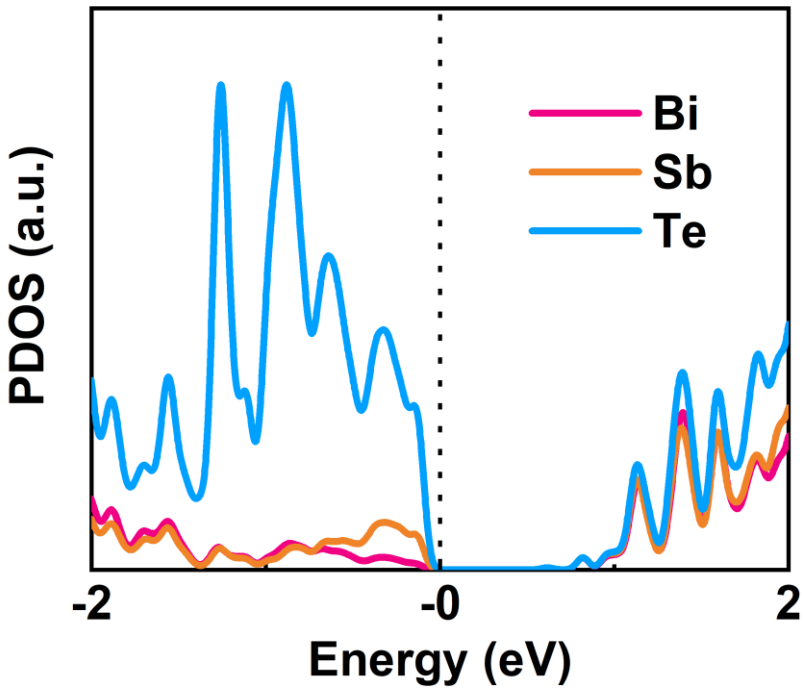

Figure S24 PDOS for $Bi_{0.778}Sb_{1.333}Te_3$.

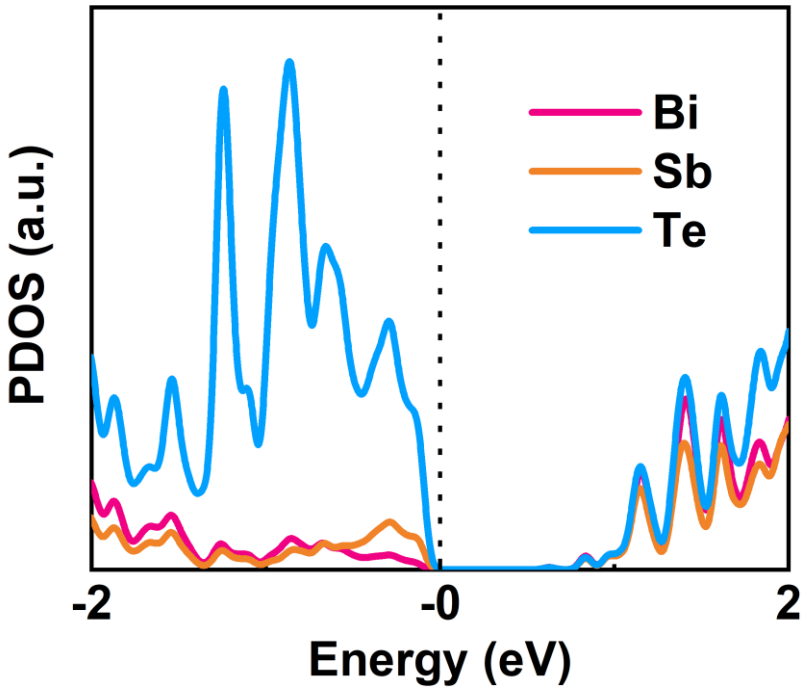

Figure S25 PDOS for $Bi_{0.889}Sb_{1.111}Te_3$.

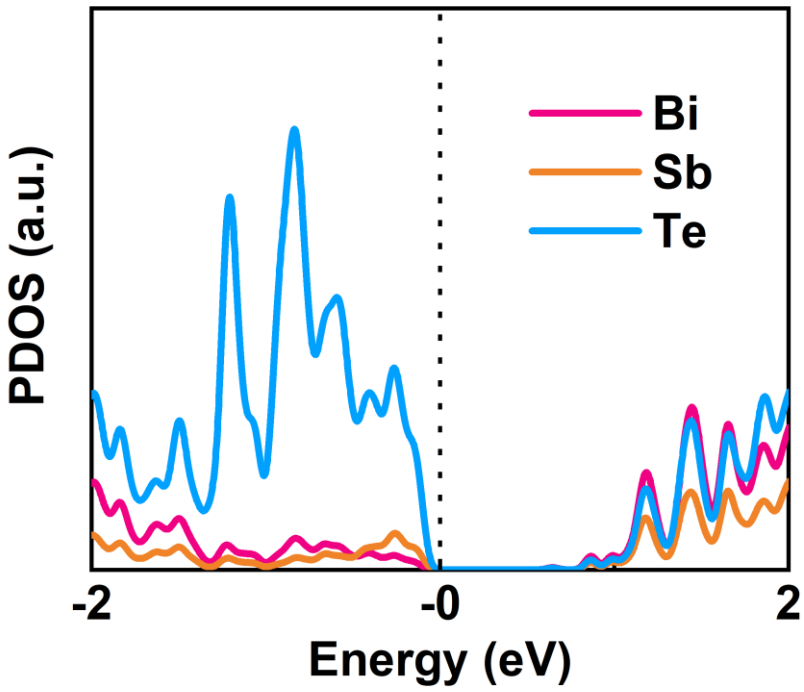

Figure S26 PDOS for $Bi_{1.111}Sb_{0.889}Te_3$.

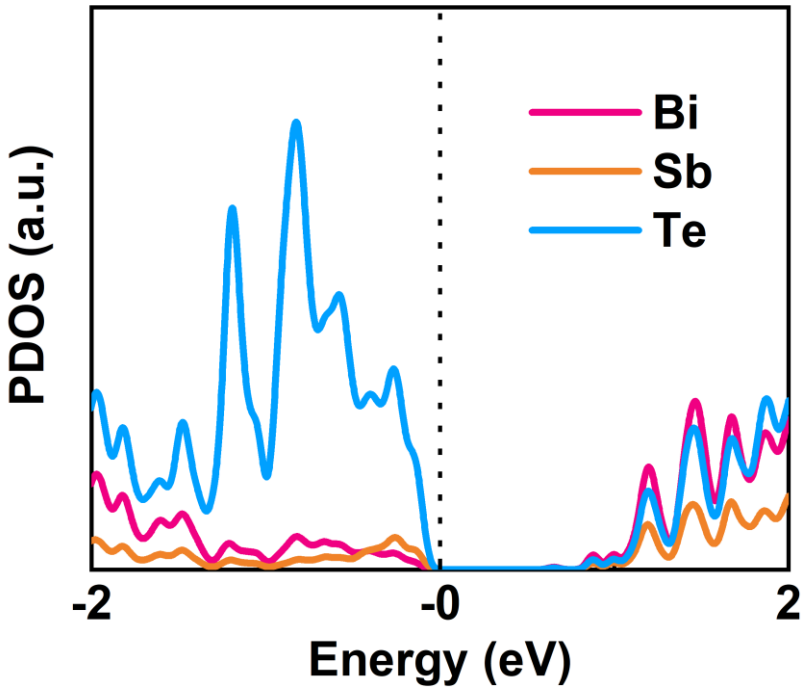

Figure S27 PDOS for $Bi_{1.222}Sb_{0.778}Te_3$.

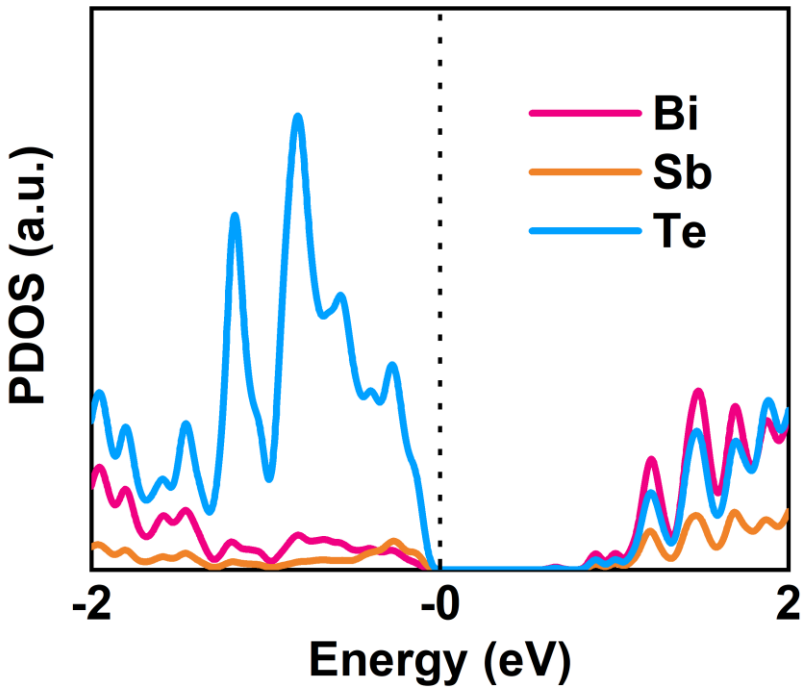

Figure S28 PDOS for $Bi_{1.333}Sb_{0.667}Te_3$.

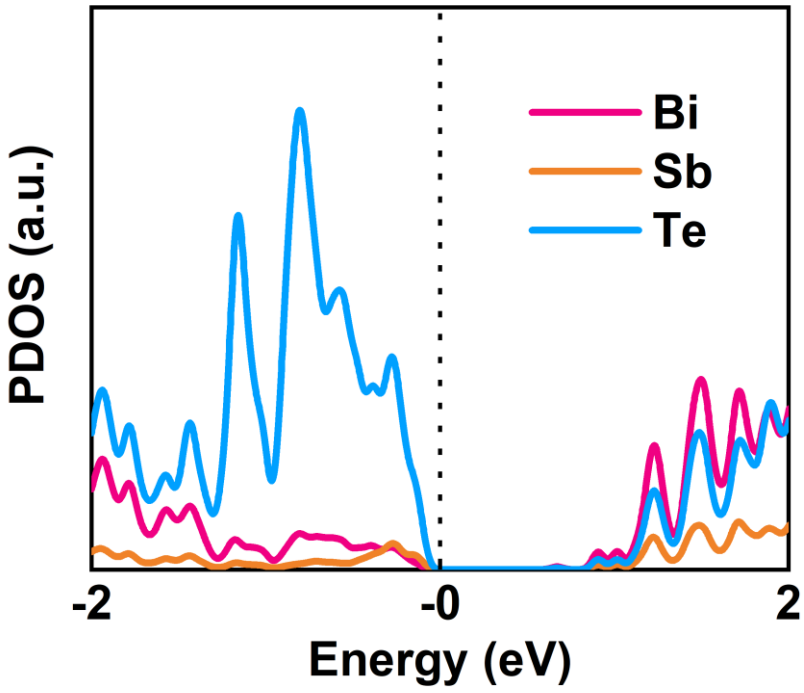

Figure S 29 PDOS for $Bi_{1.444}Sb_{0.556}Te_3$.

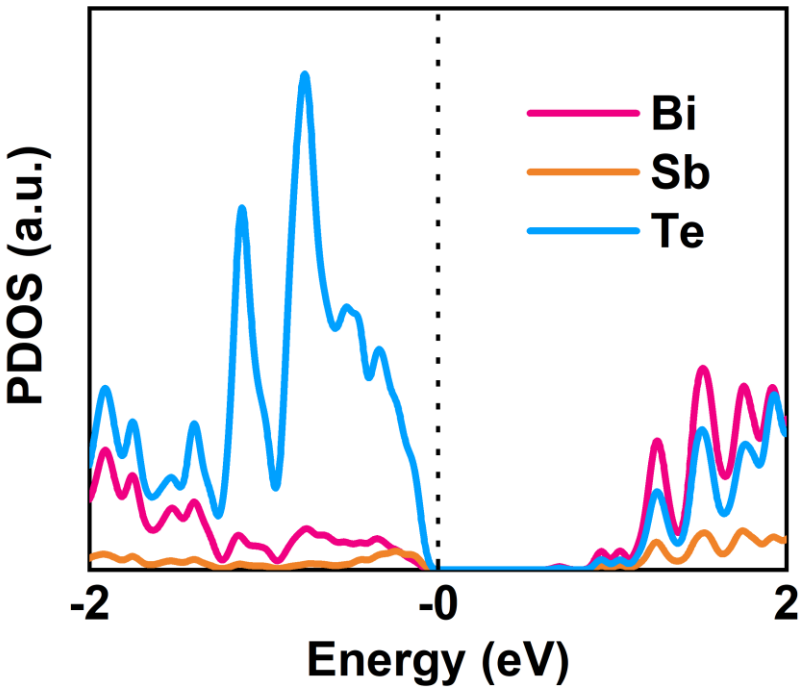

Figure S30 PDOS for $Bi_{1.556}Sb_{0.444}Te_3$.

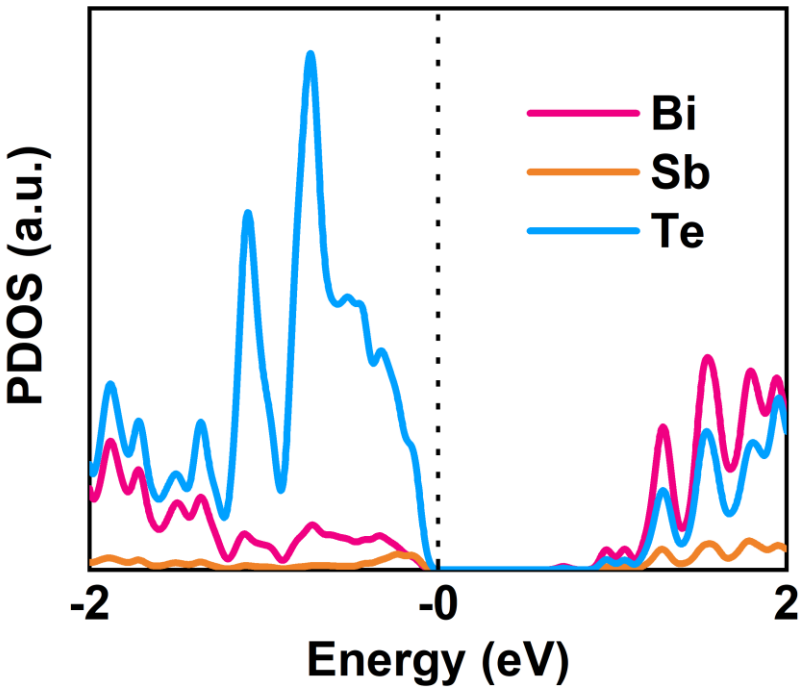

Figure S31 PDOS for $Bi_{1.667}Sb_{0.333}Te_3$.

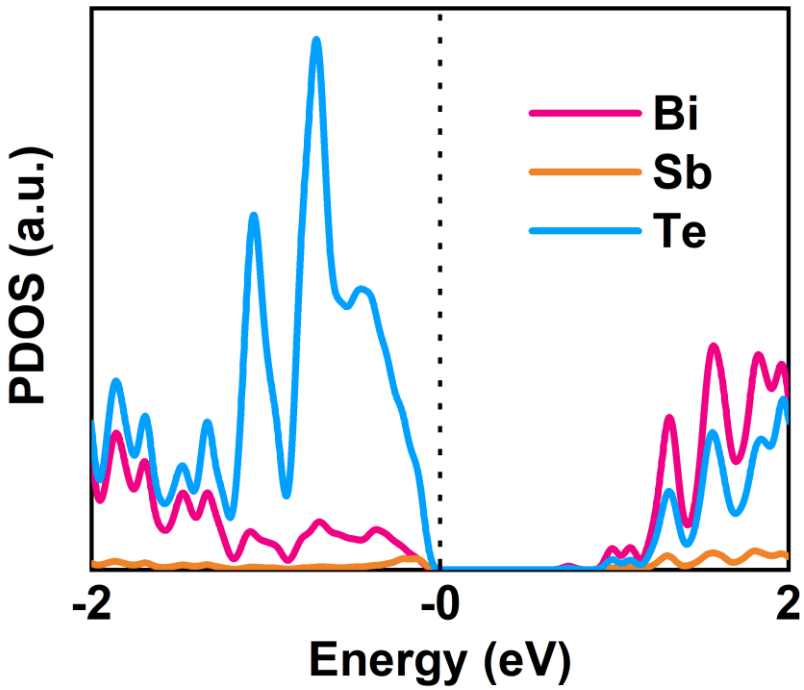

Figure S32 PDOS for $Bi_{1.778}Sb_{0.222}Te_3$.

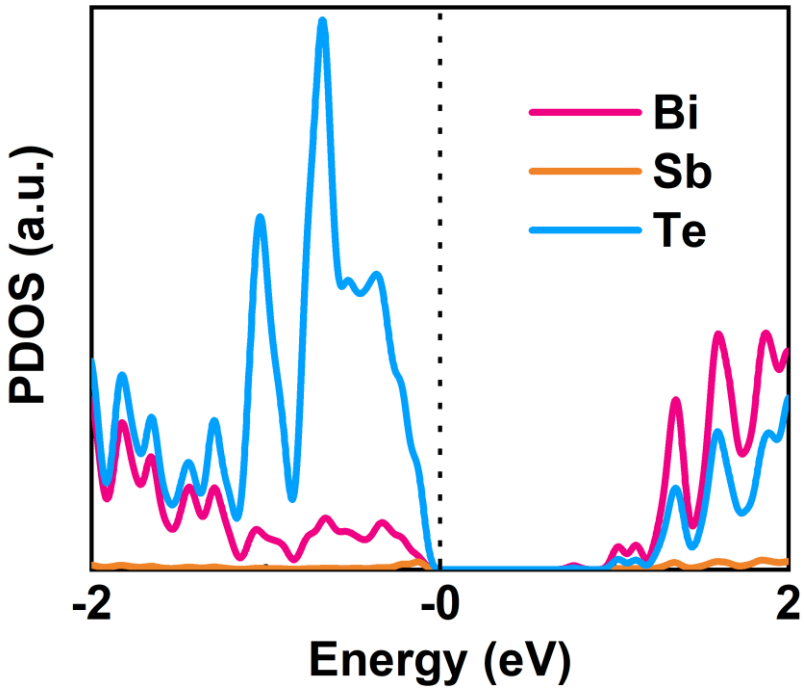

Figure S33 PDOS for $Bi_{1.889}Sb_{0.111}Te_3$.

7. The electrical conductivity and electronic thermal conductivity of BST single QLs.

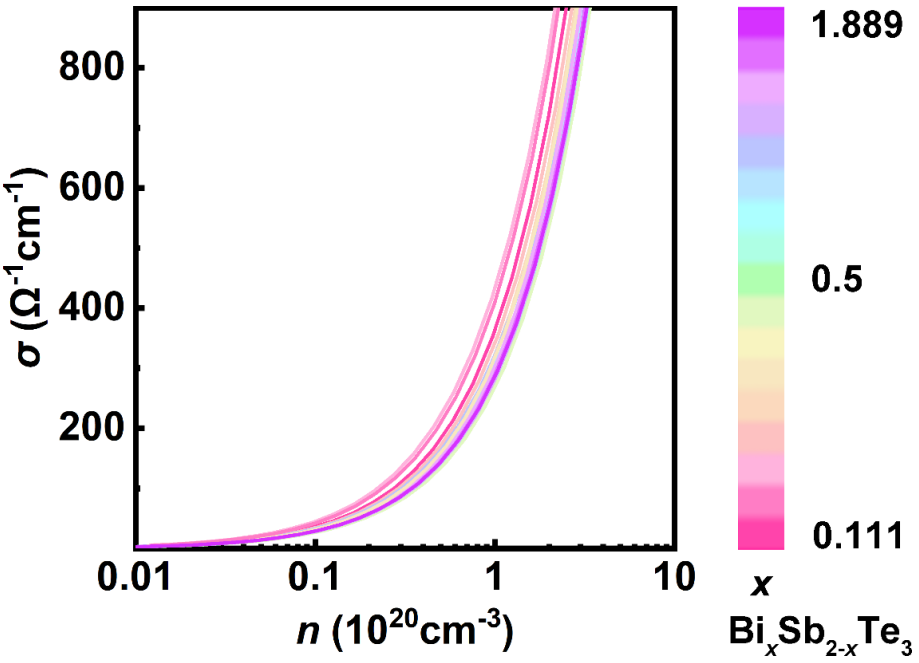

Figure S34 The electrical conductivity for *p*-type $Bi_xSb_{2-x}Te_3$ single QLs at 300 K as a function of carrier concentration.

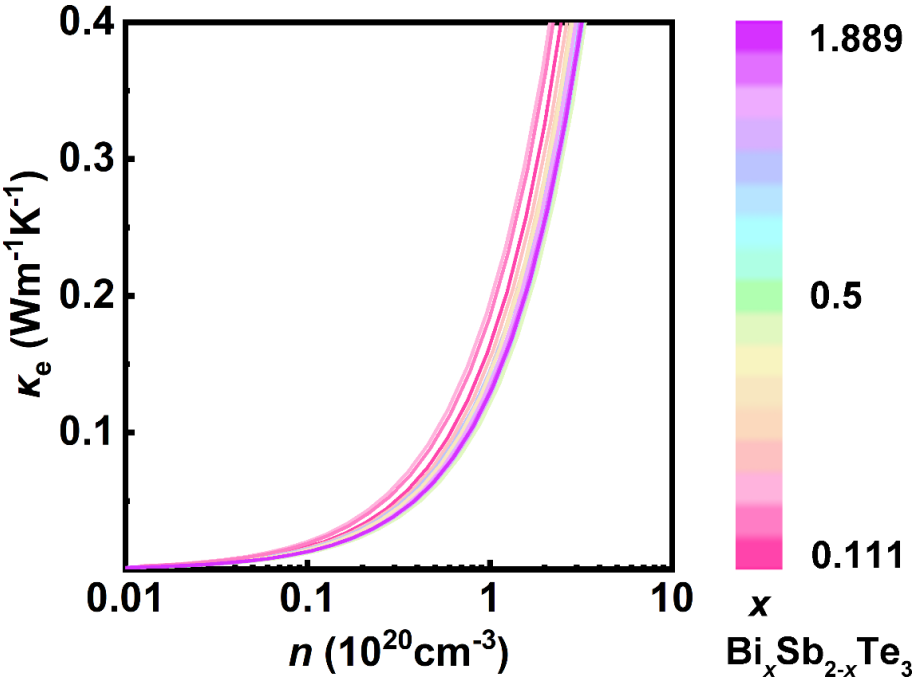

Figure S35 The electronic thermal conductivity for *p*-type $Bi_xSb_{2-x}Te_3$ single QLs at 300 K as a function of carrier concentration.